Enhancing the Protection of Shielded Thermal Protection Systems in Sample Return Spacecraft Against MMOD Impact

William Schonberg (wschon@mst.edu)
Civil Engineering Department, 1401 N. Pine Street, Missouri S&T, Rolla, MO 65409
Michael Squire (michael.d.squire@nasa.gov)
NASA Engineering and Safety Center, NASA Langley Research Center, Hampton, VA 23681
Joel Williamsen (jwilliam@ida.org)
Institute for Defense Analyses, 730 East Glebe Road, Arlington, VA 22305
Robert Stellingwerf (rfs@swcp.com)
Stellingwerf Consulting, 11033 Mathis Mountain Road SE Huntsville AL 35803
Darrel Robertson (darrel.k.robertson@nasa.gov)
NASA Ames Research Center, Moffett Field, CA 94035

Abstract

Sample return missions seek to collect samples from planets, moons, asteroids, and other planetary bodies and return them to earth for in-depth analysis. Backward planetary protection requirements are often in place for such missions to prevent the introduction of any extra-terrestrial material into the Earth's biosphere, which could occur if a meteoroid or space debris particle were to damage a critical part of the returning spacecraft. The ability of a shielding system used to mitigate this damage risk is typically characterized by a ballistic limit equation (BLE), which predicts whether or not a protected system or structural element will sustain a critical failure due to a high-speed impact. In this paper, we develop a particle-impact-based BLE for the thermal protection system (TPS) of a sample return spacecraft that is protected by a multi-

shock shield. The predictions of the BLE we develop for TPS failure are shown to be consistent with the predictions of hydrocode simulations.

Introduction

The objective of sample return missions is to collect material from planets, moons, asteroids, and other planetary bodies and return it to Earth for analysis. For example, the Mars Sample Return (MSR) campaign is a series of missions to deliver samples of Martian soil and atmosphere back to Earth. Backward planetary protection (BPP) requirements are in place for the MSR campaign to prevent the introduction of any uncontained, unsterilized Martian material—including any possible Martian microorganisms—into the Earth's biosphere. A detailed accounting of the steps being taken by NASA and ESA to ensure a successful BPP outcome is presented by Cataldo, et al (2024).

One element of BPP planning for the MSR campaign is to protect the Earth Entry System (EES) from micrometeoroids and orbital debris (MMOD) in order to help provide secure containment of the samples all the way to the Earth's surface. The mission concept back in 2021 called for a thinner TPS and cameras located in the space between a protective shield (whose construction and configuration were, at that time, still to be determined) and the TPS to inspect the TPS prior to earth entry. The TPS and the shield would have been designed to meet a typical 3-sigma mission reliability (estimates of the 2021 design were failure odds of approx. 1 in 400), and the cameras would ensure that no large impacts had punched any critical damage in the TPS. If it were determined that critical TPS damage had occurred, earth entry would have been aborted.

There were two problems with this approach. The first stemmed from the need to

accurately determine the depth of damage from a surface inspection by the cameras. This effort was compounded by the intended design of the TPS, which was supposed to made out of woven material. Early high speed impact testing of such materials revealed that they tend to have tufts of fibers sticking out of craters created by such impacts. With the intended 2021 design, impacts on the TPS were almost guaranteed (original estimates had approximately ten such impacts during the mission), although none were expected to be critical.

The second problem was that the reliability of the cameras was quite low, which required significant redundancy despite there not being a lot of room between the TPS and the shield. Furthermore, if a camera detected a crater below it in the TPS, it may well be that the camera was also hit by the meteoroid, or its fragments, on the way to impacting the TPS. This would bring into question not only the operational reliability of the camera, but also whether or not, or to what extent, the camera impact may have affected the ultimate extent of the TPS damage it, and other cameras nearby it, had recorded.

As a result of these (and other) considerations, in early 2022 the MSR Program decided that it would be more prudent to take the mass allocated to the cameras and put it into increasing the resiliency of the TPS and the shielding surrounding the EES. In so doing, although the reliability of the system was considerably increased, that came at the expense of not having a system to verify that critical damage had not occurred. But since that increased reliability resulted in system design having a failure probability on the order of 1.0E-05, a verification system was deemed unnecessary. In the end, without cameras or detection systems, the focus of the protection framework quickly turned to preventing MMOD particles from either perforating the sample containment vessels or causing enough damage to the EES thermal protection system (TPS) that would result in the EES breaking up during entry (and potentially dispersing the

samples into the atmosphere). Additional information regarding the EES as well as other components and spacecraft that are part of the MSR campaign can be found in Sarli, et al (2024).

Since there are no cameras or detection systems on board the EES, and there is no way of knowing if critical damage had occurred following a meteoroid impact, there is no action that can be taken in the event of TPS damage beyond an acceptable level, in an attempt to, for example, avoid total mission failure. As noted previously, if the TPS were to be damaged beyond an acceptable level and the EES could not survive either the return trip to earth or atmospheric entry, it would likely break up on entry and then possibly disperse the material contained in the sample container. Given mission design constraints, the only way to increase the safety of this mission and to prevent that from happening would be to enhance the shielding, but this comes with the trade-off of increased mass. Of course, the MMOD risk requirements for the MSR campaign are much more stringent than most science missions, which are only concerned with mission success. Tight BPP requirements necessitate a very low acceptable MMOD risk of damage to the TPS, which in turn drives the shield design.

The desired extra level of protection for the EES can be attained by placing a robust MMOD shield standing off at a small distance away from the TPS on the sample return capsule. This shielding would protect the TPS against damage from MMOD impacts and would be removed just prior to the capsule's entry into the Earth's atmosphere. The protective ability of any such shielding system is typically characterized by a ballistic limit equation (BLE), which predicts whether or not a protected system or structural element will sustain a critical failure following an MMOD impact.

The concept of shielding a particularly sensitive or critical spacecraft component from the hazards of the MMOD environment has been studied extensively since it was first proposed

nearly eighty years ago. Over that time period, BLEs have been developed for a variety of shielding systems, based on the level of protection desired and the anticipated exposure of the spacecraft to the MMOD environment. Schonberg (2016), for example, presents a history of the development of the BLEs frequently used in the design of long-duration spacecraft, such as the International Space Station. However, until very recently, protecting the contents of a spacecraft by shielding its outer blanket of TPS had yet to be explored, and general BLEs for this type of system had yet to be developed.

In one of the first studies on shielded TPS under high-speed impact, Williamsen, et al (2022) developed a crater depth prediction equation for TPS protected by a foam-filled Whipple Shield using hydrocode data for a variety of shield thicknesses and locations above the TPS. The equation developed was seen to able to successfully model numerical predictions of penetration depth for a variety of projectile densities and Whipple Shield configurations. In a parallel effort, Schonberg and Squire (2024) developed a general BLE for a variety of similar shield+TPS configurations under similar impact conditions. That BLE was shown to accurately predict the failure or non-failure of a Whipple Shield+TPS system when the failure criterion was through-perforation of the TPS.

As new materials have been developed and certified for space and aerospace applications, Whipple Shields constructions have steadily evolved to take advantage of any increases in protective ability that these new materials might have been able to provide (see again, Schonberg, 2016). Multi-shock shields were originally developed in the early 1990s to significantly improve the protection afforded a long-duration spacecraft against MMOD impacts over a simple Whipple Shield. These shields typically have several layers of a ceramic fiber standing off at small distances from each other, with the spaces between them either empty or

filled with a polymer foam.

Following on the initial efforts by Williamsen and Schonberg that studied the response of a blanket of TPS protected by a Whipple Shield, the next step, then, was to perform similar studies using multi-shock shield configurations as the protective devices. Corbett, et al (2024) were able to successfully apply the techniques used in Williamsen, et al (2022) to develop a similar TPS penetration depth predictor equation using hydrocode data for TPS protected by a multi-shock shield. And so, in a manner analogous to the process used by Schonberg and Squire (2024), in this paper we develop a particle-impact-based BLE for TPS protected by a multi-shock shield.

We develop this BLE so that it, like the BLE developed by Schonberg and Squire (2024), can be used for a variety of impact scenarios, as well as various multi-shock shield component materials and geometries. The predictions of this BLE regarding whether or not a TPS failure would occur are seen to be consistent with the predictions of hydrocode simulations upon which it is based. As such, sample return campaign developers are now able to consider using such a shield in the design of the returning spacecraft in order to meet spacecraft BPP requirements.

BLE Development—Configurations, Material Properties, and Impact Conditions

Figure 1 shows a sketch of a multi-shock shield + TPS system that is impacted by a projectile with diameter d_p at a velocity V_p. The multi-shock shield consists of alternating layers of a shocking material (thickness t_b) —hence the term "multi-shock shield"—a foam filler (thickness ΔS), and ending with a final layer of material (identified in Figure 1 as the "rear wall") having a thickness t_w. Each additional layer of shocking material and foam filler increases the protective ability of the multi-shock shield. The TPS (thickness t_{TPS}) is attached to a substructure

of some kind; for the purposes of this study, the effect of that substructure on the impact response of the TPS is ignored.

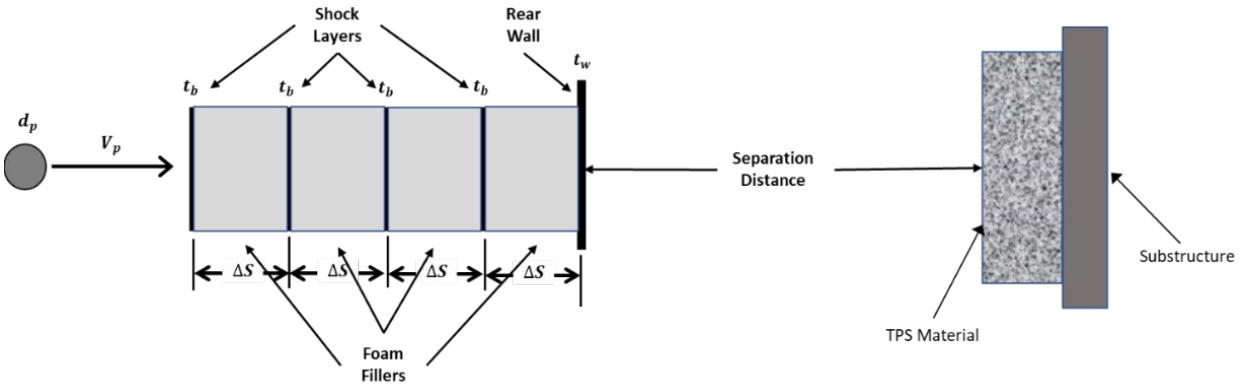

Fig. 1. Sketch of the Multi-Shock Shield+TPS System (Elements and Distances Not to Scale)

Following the impact of the projectile on the outer shocking layer (aka the "bumper"), a debris cloud consisting of projectile and bumper fragments travels through the shield and eventually impacts the underlying TPS, creating craters in the TPS having a maximum penetration depth of d_{pen}. This depth of penetration is one of the measures that is frequently used to assess the remaining protection provided by the TPS. Hence, if the penetration depth were to exceed a maximum allowable fraction of total TPS thickness, the TPS would be considered in a "failed" state. Likewise, if the penetration depth were less than the maximum allowable, the TPS would be considered to be "not failed," that is, it would still be able to provide an adequate level of thermal protection to the spacecraft. BLEs developed for these types of configurations are typically related to some specified maximum allowable TPS penetration depth criterion, which may or may not include some portion of the support substructure beneath it (i.e., the criterion includes complete penetration of the TPS thickness). As will be seen later, the BLE developed herein does not include the effects of the substructure under the TPS.

Results from 14 high-speed impact tests and 286 numerical simulations with various impact conditions, shield thicknesses and materials, separation distances, filler thicknesses and

materials, and rear-wall thicknesses and materials were used to support the development of the multi-shock shield + TPS BLE (hereafter referred to as the MSS+TPS BLE). The numerical impact simulations were performed using the Smooth Particle Hydrodynamic Code (SPHC) and the Arbitrary Lagrangian-Eulerian Three-dimensional (ALE3D) hydrocodes. Details of the numerical modelling used in these hydrocode simulations can be found in Williamsen, et al (2022) and Corbett, et al (2024).

There are no experimental facilities capable of shooting projectiles of reasonable size at the energies and velocities that would be required to allow experimental verification of the performance of the MMOD shield and TPS against meteoroids to the risk level desired (i.e., projectiles at ~1cm diameter, velocities at 30–50 km/s). Traditional risk methodology uses experiments at ~7 km/s and then assumes equal energy impacts cause equal damage, and uses this to extrapolate to higher impact velocities. This scaling method is known to be excessively conservative, but has been acceptable for missions meeting 2 or 3 sigma risk levels. For the MSR Campaign, where the target risk level is 1 in 100 000 to 1 in a million, this would result in unnecessarily heavy TPS and meteorite shielding.

The hypervelocity impact tests were performed using the light gas guns (LGGs) at the NASA White Sands Test Facility (WSTF) Remote Hypervelocity Test Laboratory (RHTL); in most cases, the 17-caliber LGG was used. Projectile velocity was obtained in each test using either a laser station consisting of two multi-beam lasers and a muzzle laser that is paired with either laser station, or with photo diode impact flash detectors, that are located at the stripper plate and at the target impact point. This results in an impact velocity measurement with only 1-2% measurement uncertainty. Projectile integrity was verified using ultra-high-speed imaging system cameras to capture shadowgraphs of the projectiles in flight immediately prior to impact

183 (the typical setup captures a shadowgraph of the projectile). The pressure within the target
184 chamber was typically kept below 15 torr (~0.3 psia) using nitrogen gas in order to minimize the
185 effects of oxygen during impact.
186 The ability of SPHC and ALE3D to model high-speed impact events involving a variety
187 of targets and to provide realistic predictions of hypervelocity impacts within and beyond the
188 testable regime has been shown in a number of studies, including those by Stellingwerf (1990),
189 Stellingwerf and Wingate (1994), and Williamsen, et al (2022) for SPHC, and Gerassimenko
190 (1998), Wilbeck, et al (2001), and Miers, et al (2020) for ALE3D.
191 With regard to the ability of SPHC to correctly model these types of impact events, a
192 previous study performed by Schonberg and Williamsen (2023) compared x-ray images of debris
193 clouds created in a high-speed impact and the debris clouds predicted by SPHC. That study
194 showed that SPHC performs very well when predicting impact response at impact velocities
195 attainable by a light gas gun. Furthermore, Williamsen, et al (2022) compared the predictions of
196 crater depths and diameters by SPHC to impact test results using a TPS consisting of 3D woven
197 carbon and nylon phenolic fibers. The SPHC simulations modelled this TPS construction by
198 using alternating carbon fiber and nylon fiber layers, and simulated the porosity of the material
199 by randomly omitting ~20% of the SPH particles in each of these layers. Comparisons of the
200 SPHC crater morphologies and experiments results showed excellent agreement. Beyond that,
201 the code has been used at higher velocity impacts (up to 22 km/s), and its predictions of crater
202 geometries have compared favorably to those of the craters generated by the Los Alamos Van de
203 Graff accelerator. Wingate, et al (1993) review the results of a number of additional validation
204 activities in this impact velocity regime.
205

With regard to ALE3D, it is important to note that in order to be able to obtain more accurate estimates of the cratering, it is necessary to take into account the strength and phase change of the materials. Latent heats of melting and vaporization are important energy sinks at >10 km/s impacts, and vaporized material spreads out more rapidly, thereby causing less damage to lower target layers. Hypervelocity impacts result in shock pressures well above the Hugoniot elastic limit, so crater morphologies predicted by ALE3D tend to be hemispherical as the shock wave expands, pushing material away from the impact location. As the shock expands it decays as $1/r^2$ (where r is the distance from the source)until the strength of the material is able to withstand the shock wave remnants, which means strength is still important in determining final crater size.

Material models in ALE3D exhibit strain-rate hardening (see, e.g., Noble, et al, 2017), so impacted materials appear harder under hypervelocity impact than they do under quasistatic tests. In ALE3D, then, strength is given as a function of strain rate; however, for the ALE3D simulations performed in support of BLE development, the strength was not allowed to exceed the experimentally determined values from impacts at 7 km/s. Freezing the strength at the level to match 7 km/s experiments and not extrapolating beyond experiment did provide some conservatism to the ALE3D simulations. By combining strength models and equations of state that capture latent heats of melting, vaporization, and ionization, ALE3D was able to make reasonably accurate predictions of damage from meteoroid impacts.

It is also important to note that neither SPHC or ALE3D were used or run to pinpoint the precise impact parameters that would result in an exact determination of a ballistic limit impact event. This then avoided any of the difficulties that might be encountered by either code when attempting to model impact scenarios when material strengths cease to play prominent roles in

response modelling. Rather, for a given impact velocity, impact simulations were run using successively increasing projectile diameters until target failure occurred (if the first run resulted in a non-failure event), or increasing decreasing projectile diameters until target failure no longer occurred (if the first run resulted in a failure event). The ballistic limit diameter for that particular impact velocity was then taken to lie between the two successive diameters that did and did not result in target failure.

Taken together, all of the above considerations provide us with confidence in the validity of using these hydrocodes to provide the data needed to develop the BLE presented in this paper.

Tables 1 and 2 present a summary of the material properties and the MSS+TPS configurations used in the hypervelocity impact test programs and hydrocode simulations. In keeping with previous BLE development activities, material strength units are ksi; subsequent use of this parameter in one of the BLE component equations requires the material strength term to be entered in ksi as well. Additionally, Table 3 presents a summary of the impact conditions for both the impact tests and the hydrocode simulations.

In Tables 1 and 2, "T300/Ep" and "T300/RS3C" refer to rigid composite walls made of T300 graphite fibers embedded in two different epoxy matrix materials, while "IM7/977-3" and "KM2/Ep" refer to rigid composite walls made of either IM7 graphite fibers or KM2 Kevlar fibers embedded in an epoxy matrix. Details of the composite fiber including orientation, number of layers, etc., were not considered as part of this study. Also, because the TPS composition and thickness were held constant, the BLE developed herein is only valid for the composition and thicknesses shown in Tables 1 and 2. Lastly, note that the "Rear Wall" in Tables 1 and 2 refers to the final bumper in the multi-shock shield (see Figure 1), not the substructure outer wall.

Table 1. Materials and Geometric Parameters for
Multi-Shock Shield + TPS System Configurations Used in Testing

Configuration	Layup M9a	Layup M9b	Layup M14a	Layup M14b	Layup M14c	Layup M14d	Units
Outer Bumpers	Nextel	Nextel	Nextel	Nextel	Nextel	Nextel	-----
Bumper Thickness	0.28	0.28	0.28	0.28	0.28	0.28	mm
Density	0.857	0.857	0.857	0.857	0.857	0.857	g/cm^3
No. of Bumpers	4	4	4	4	6	5	-----
Gap Material	Solimide	Solimide	Solimide	Solimide	Solimide	Solimide	-----
Gap Thickness	13	13	13	13	13	13	mm
Gap Material Density	0.0056	0.0056	0.0056	0.0056	0.0056	0.0056	g/cm^3
No. of Gaps	4	4	4	4	6	5	-----
Rear Wall	T300/Ep	T300/RS3C	KM2/Ep	KM2/Ep	KM2/Ep	KM2/Ep	-----
Thickness	0.914	0.876	2.134	1.067	1.422	0.711	mm
Density	1.5	1.5	1.3	1.3	1.3	1.3	g/cm^3
Strength	264	264	347	347	347	347	ksi
Total Shield Thickness	5.40	5.40	5.525	5.419	8.110	6.711	cm
Total Shield Areal Density	0.264	0.259	0.403	0.264	0.373	0.249	g/cm^2
Average Shield Density	0.0489	0.0480	0.0728	0.0487	0.0459	0.0371	g/cm^3
Stand-off to TPS	10	10	10	10	10	10	cm
TPS Material	HEEET-IL*	HEEET-IL*	HEEET-IL*	HEEET-IL*	HEEET-IL*	HEEET-IL*	-----
TPS Thickness	1.44	1.44	1.44	1.44	1.44	1.44	cm
TPS Material Density	0.83	0.83	0.83	0.83	0.83	0.83	g/cm^3

*HEEET=Heatshield for Extreme Entry Environment Technology

Examination of the configuration specifics in Tables 1 and 2 reveals that there are some differences between the designs of the systems used in testing and the designs of the systems used in the hydrocode runs. This was done for two reasons: (1) this would allow for the study, if desired, of the effects of small variations in system design on system response, and (2) this would facilitate the development of a BLE that would be applicable for a much wide ranges of system designs. Of the configurations listed in Tables 1 and 2, however, it is evident that Layup 1 is most similar to Layups M9a and M9b, Layup 2 is most similar to Layup M14a, and Layup 3 is most similar to Layup M14b.

Table 2. Materials and Geometric Parameters for Multi-Shock Shield + TPS System Configurations Used in Numerical Simulations

Configuration	Layup 1	Layup 1.6	Layup 2	Layup 3	Layup L3.3.C	Units
Outer Bumpers	Nextel	Nextel	Nextel	Nextel	Nextel	-----
Bumper Thickness	0.28	0.28	0.28	0.28	0.28	mm
Density	0.857	0.857	0.857	0.857	0.857	g/cm^3
No. of Bumpers	4	6	4	4	3	-----
Gap Material	Solimide	Solimide	Solimide	Solimide	Solimide	-----
Gap Thickness	13	13	13	13	35	mm
Gap Material Density	0.0056	0.0056	0.0056	0.0056	0.0056	g/cm^3
No. of Gaps	4	6	4	4	3	-----
Rear Wall	IM7/977-3	IM7/977-3	KM2/Ep	KM2/Ep	IM7/8552-1	-----
Thickness	0.786	0.786	1.8	0.9	1.46	mm
Density	1.54	1.54	1.3	1.3	1.54	g/cm^3
Strength	398	398	347	347	398	ksi
Total Shield Thickness	5.391	8.047	5.492	5.402	10.730	cm
Total Shield Areal Density	0.246	0.309	0.359	0.242	0.356	g/cm^2
Average Shield Density	0.0457	0.0384	0.0654	0.0448	0.0331	g/cm^3
Stand-off to TPS	10	10	10	10	10	cm
TPS Material	HEEET-IL	HEEET-IL	HEEET-IL	HEEET-IL	HEEET-IL	-----
TPS Thickness	1.44	1.44	1.44	1.44	1.44	cm
TPS Material Density	0.83	0.83	0.83	0.83	0.83	g/cm^3

Table 3. Impact Conditions for High-Speed Impact Tests and Hydrocode Simulations

Impact Parameter	High-Speed Impact Tests	Hydrocode Simulations	Units
Projectile Material	Aluminum	Ice, Porous Ice, Aluminum, Granite Dunite, Iron	-----
Projectile Diameter	5 – 7	3 – 15	mm
Impact Velocity	6.9 – 7.1	7, 15, 25, 30 40, 55, 70	km/s
Trajectory Obliquity*	0	0, 30, 45	deg

*measured from target normal

BLE Development—Process Overview

The MSS+TPS BLE was developed to be applicable for impact velocities up to 60 km/s, for projectile material densities ranging from that of water (1.0 g/cm^3) to steel (8.0 g/cm^3), and for normal as well as non-normal impacts. Furthermore, the BLE was developed to be flexible enough so that it can be used for parametric and design trade studies (i.e., it was written in terms of as many MSS+TPS system parameters as possible). As is the case in nearly every BLE developed for multi-wall targets, the MSS+TPS BLE has three regions: a low-velocity regime, a high-velocity regime, and a middle segment that is a linear (typically) interpolation between the ending point of the low-velocity regime and the starting point of the high-velocity regime as in the NNO BLE developed by Christiansen (2019), for example.

The MSS+TPS BLE was initially developed using only aluminum projectiles in the hydrocode simulations. That initial form was subsequently modified based on test results at impact velocities near 7 km/s; additional terms and exponent functions were subsequently added to account for other projectile materials based on results obtained using the SPHC and ALE3D hydrocodes. Details regarding this process and the final form of the MSS+TPS BLE are given in the following section.

The MSS+TPS BLE

Following the process summarized above, the MSS+TPS BLE was developed in the following two phases.

Phase One: Develop the terms of the core MSS+TPS BLE.

The form of the core MSS+TPS BLE was based on the form of the core BLE previously used by Schonberg and Squire (2024) in their development of the WS+TPS BLE. In this particular exercise, the BLE was developed assuming through-perforation of the TPS as the

failure criterion, for aluminum projectiles impacting the MMS+TPS targets at obliquities of 30 deg, a stand-off distance from the rear of the multi-shock shield to the TPS of 10 cm, and a TPS thickness of 14.4 cm. The construction and parameters of the multi-shock shields were varied for the shield layups and configurations shown in Tables 1and 2.

A pair of equations was subsequently developed, one for the lower-velocity regime and one for the higher-velocity regime, which, together with the linear interpolation segment between these two regimes, formed the core BLE that spanned the entire impact velocity regime of interest. Each of the low-velocity and high-velocity equations was of the form:

$$d_{crit} = A * V_p^B * cos^C \theta_p \quad (1)$$

This BLE calculates the critical diameter (d_{crit}), which is the diameter of the smallest particle that will cause damage exceeding the failure criterion, as a function of particle velocity (V_p) and impact angle from normal (θ_p). The initial values of the constants A, B, and C in Eqn (1) were determined using the following process, assuming that the impacting projectile will perforate the forebody shield and some remnant of it continues forward to impact the TPS:

- Step 1: Calculate the size and speed of largest fragment exiting the forebody multi-shock shield. This is accomplished by modeling the multi-shock shield as a single aluminum plate with a thickness that yields the same areal density as the original multi-shock shield, and then using equations for a thin-plate impact developed by Schonberg and Williamsen (2023) to determine the largest fragment size expected to exit the multi-shock shield and its speed.
- Step 2: Calculate the depth of penetration of that largest fragment into the TPS. This is accomplished using an appropriate empirical TPS penetration depth predictor equation, such as that developed by Libben, et al (2019) for HEEET-IL, which is

319 modified to replicate the following trends observed in SPHC predictions and results
320 from 7 km/s impact velocity tests:
321 - Penetration depth grows quickly with increases in projectile diameter for a 7 km/s
322 impact velocity, but not as quickly for higher velocities; and
323 - This trend is more pronounced in normal impacts than in oblique impacts, and for
324 the shields with higher areal densities.
325 • Step 3: Compare calculated TPS penetration depths from Step 2 against the stated
326 maximum depth to assign a penetration or no penetration (P/NP) value to each
327 impact, and then noting at which projectile diameter the TPS penetration begins to
328 exceed this maximum value.
329 • Step 4: Adjust the values of A, B, and C in Eqn (1) to improve the placement of the
330 BLE among the P/NP data based on visual inspection of how the curve generated by
331 the BLE captures the data. Ideally, hydrocode predictions or test results indicating
332 TPS failure (i.e., penetration) should be above the BLE, while predictions or test
333 results indicating non-failure (i.e., no penetration) should be below the BLE.

334 Modifications to the initial values of the parameters A, B, and C in Eqn (1) were made in
335 the next phase of this process after adding target, projectile, and impact parameters to the core
336 BLE as discussed below.

337 *Phase Two: Extend the core MSS+TPS BLE to account for projectile materials other than*
338 *aluminum and trajectory obliquities other than 30 deg.*

339 This was accomplished by modifying the parameters A, B, and C in each of the core BLE
340 segments (i.e., low velocity and high velocity), and expressing the parameters as functions of
341 system geometries (e.g., thicknesses) and material properties (e.g., densities) as well as impact

parameters (e.g., projectile densities, trajectory obliquities). These functions were again determined by ensuring that plots of the resulting MSS+TPS BLE would, to the greatest extent possible, pass in between hydrocode predictions of TPS failure and non-failure.

This process of plotting, checking, and reworking the parameter functions for a better fit to the hydrocode data also required an adjustment to the impact velocity value at which began the high velocity regime of the BLE (i.e., V_H), and to the impact velocity exponents as well in order to ensure a better fit to the hydrocode data. When the parameter values of A, B, and C in the core MSS+TPS BLE were replaced by these parameter functions, the resulting BLE became applicable to a much wider range of projectile materials and impact trajectory obliquities.

In the end, the following equations were obtained for the low- and high-velocity portions of the MSS+TPS BLE:

(1) Low velocity regime ($0 < V_p < 7.0$ km/s):

$$d_{crit} = 0.95 * LVMF * g_L * f_L * h_L(\rho_p, \theta_p) * V_p^{f_{VL}} cos^{f_{THL}}\theta_p \quad (2)$$

(2) High velocity regime ($V_p > V_H(m_b, \sigma_{rw}, t_{MS}, \theta_p)$ km/s):

$$d_{crit} = 0.95 * HVMF * k_H * f_H * h_H(\rho_p, \theta_p) * V_p^{f_{VH/VPRF}} cos^{f_{THH}}\theta_p \quad (3)$$

where d_{crit} is the critical particle diameter (in cm) and V_p is the impact velocity (in km/s). Between the two transition velocities (i.e., for $7.0 \text{ km/s} < V_p < V_H$ km/s), d_{crit} is the linear interpolation between the d_{crit} value at $V_p = 7$ km/s and the d_{crit} value at $V_p = V_H$ km/s. Furthermore, in Eqns (1, 2), ρ_p is the density of the critical particle (in g/cm^3), θ_p is the trajectory obliquity measured from the outer wall normal (in radians), m_b is the areal density of multi-shock shield (in g/cm^2) including the rear wall, t_{MS} is the thickness of the entire multi-shock shield, that is, the sum of all blanket thicknesses, foam thicknesses, and the rear wall thickness (in cm), and σ_{rw} is the strength of the rear wall of the multi-shock shield (in ksi).

In Eqns (1, 2), the functions f_L, f_H and f_{VL}, f_{VH} and f_{THL}, f_{THH} take into account the number of multi-shock layers, the masses and thicknesses of the multi-shock blankets and any gap-filling foam, the mass and thickness of the rear wall, and the strength of the rear wall material. These functions all have the same following form:

$$function = A(\sigma_{rw}/100)^B \, m_b^C t_{MS}^D \tag{4}$$

where the values of the parameters A – D in Eqn (4) are given in Table 4 below.

Table 4. Parameter Values for the f Functions

	f_L	f_H	f_{VL}	f_{VH}	f_{THL}	f_{THH}
A	0.6222	1.4646	-0.2254	-0.3936	-0.1512	-0.6690
B	-0.4698	-0.6113	0.0375	-0.0179	0.1215	-0.7573
C	-0.2796	-0.6247	-0.0496	-0.0587	-0.7660	0.8669
D	0.3125	0.3081	-0.1284	-0.0808	0.0567	1.1427

The function g_L takes into account the response of heavier shields that is observed at lower impact velocities for normal and near-normal impacts. It has the following functional form:

$$g_L = 1 + (G_1 m_b + G_2 - 1) e^{-\theta_p^{0.6}/0.07} \tag{5}$$

where θ_p is in radians, with $G_1 = 1.4670$ and $G_2 = 0.6264$.

The functions $h_L(\rho_p, \theta_p)$ and $h_H(\rho_p, \theta_p)$ take into account the density of the projectile material and its effect on impact response. Each of these functions also has an impact obliquity effects term and an additional adjustment factor for ice and porous ice projectiles in the high velocity regime when $\theta_p = 0$ deg. These additional terms are necessary so that the BLE plots better fit the SPHC data for non-aluminum projectiles.

$$\begin{Bmatrix} h_L(\rho_p, \theta_p) \\ h_H(\rho_p, \theta_p) \end{Bmatrix} = 0.9387 \rho_p^{-0.5379} * \begin{Bmatrix} 1.01\left[1 - \exp\left(-\rho_p^{0.6}/0.28\right)\right] cos^{-0.605}\theta_p \\ 1.11\left[1 - \exp\left(-\rho_p^{1.2}/0.72\right)\right] cos^{-0.605}\theta_p \end{Bmatrix} * \tag{6}$$

$$\left\{\frac{1}{\left[1+\exp\left(-\rho_p^{2.5}/0.75\right)\right]cos^{1,150}\theta_p}\right\}$$

In Eqn (6), the first term on the right-hand-side of the equation can be viewed as a baseline projectile material term. The second term consists of a projectile material density and impact obliquity factors, while the third term is the high velocity adjustment factor for ice and porous ice projectiles.

We still need an expression for V_H that takes into account the observed behavior that is present in hydrocode simulations of normal and near-normal impacts. After several iterations, it was found to have the following functional form, which is a slightly modified version of Eqn (4):

$$V_H = 2 * A(\sigma_{rw}/100)^B \, m_b^C t_{MS}^D * cos^{0.33}\theta_p \qquad (7)$$

where the constants A – D in Eqn (7) are given as follows:

Table 5. Values of Constants A – D in Equation (7)

Coeff	***Value***
A	8.5623
B	-0.0491
C	-0.2703
D	0.1162

The function k_H was added following the V_H adjustment when it became evident that the BLEs consistently overpredicted the SPHC results for the 30-deg impacts (but not the 0-deg impacts). Its final form is given by

$$k_H = 0.9 + 0.1 * e^{-15\theta_p} \qquad (8)$$

where θ_p is in radians.

The *VPRF* and *HVMF* terms serve to flatten and lower, respectively, the BLEs in the high velocity regime, while the term *LVMF* makes the necessary adjustments in the low velocity regimes. These final terms are given as follows:

$$VPRF = 4.0 + 1.3 * exp\left[-\left(\sqrt{\sigma_{RW}/(m_b * t_{MS})}/20\right)^{28}/0.0008\right] \quad (9)$$

$$HVMF = 0.34 + 0.04 * exp\left[-\left(\sqrt{\sigma_{RW}/(m_b * t_{MS})}/20\right)^{28}/0.0008\right] \quad (10)$$

$$LVMF = 1 - 0.15 * \exp\left[-cos^{20}\theta_p/0.09\right] \quad (11)$$

where θ_p is again in radians. This completes the development of the MSS+TPS BLE.

Assessment of the MSS+TPS BLE

An assessment of the MSS+TPS BLE developed herein was made by comparing BLE predictions of TPS failure (P) or non-failure (NP) against hydrocode simulation results and available test results, and by noting how consistently TPS failures and non-failures as predicted by hydrocode or testing were above or below the BLE. As noted previously, the BLE was developed so that, to the greatest extent possible, hydrocode predictions or test results indicating TPS failure should be above the BLE, while predictions or test results indicating non-failure should be below the BLE.

Figures 2 – 7 present comparisons of BLE plots, hydrocode predictions and test results for various projectile materials, impact conditions, and MSS+TPS design. In these figures, hollow circles and squares indicate TPS failures, while solid circles and squares indicate non-failures; triangular markers indicate either hydrocode predictions or test results that appeared to be either on the verge of or just past the point of TPS failure (i.e., a ballistic limit impact, hence the ”BL” designation in the legends of these plots). In Figures 2 – 7, hollow markers above the BLE correspond to hydrocode runs or test results having TPS failure caused by projectiles with diameters larger than ballistic limit diameters as predicted by the BLE, and indicate successful predictions by the MSS+TPS BLE.

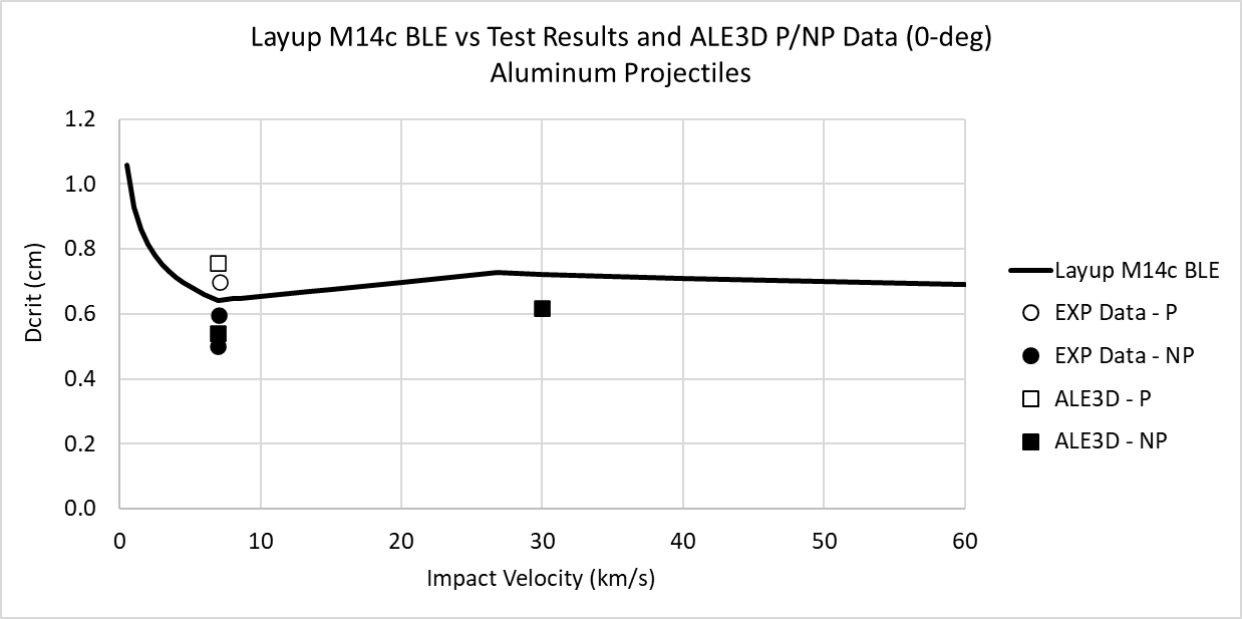

Figure 2. Comparison of MSS+TPS BLE, Experimental Results, and ALE3D Hydrocode Predictions for Layup M14c, 0-deg Impacts, Aluminum Projectiles

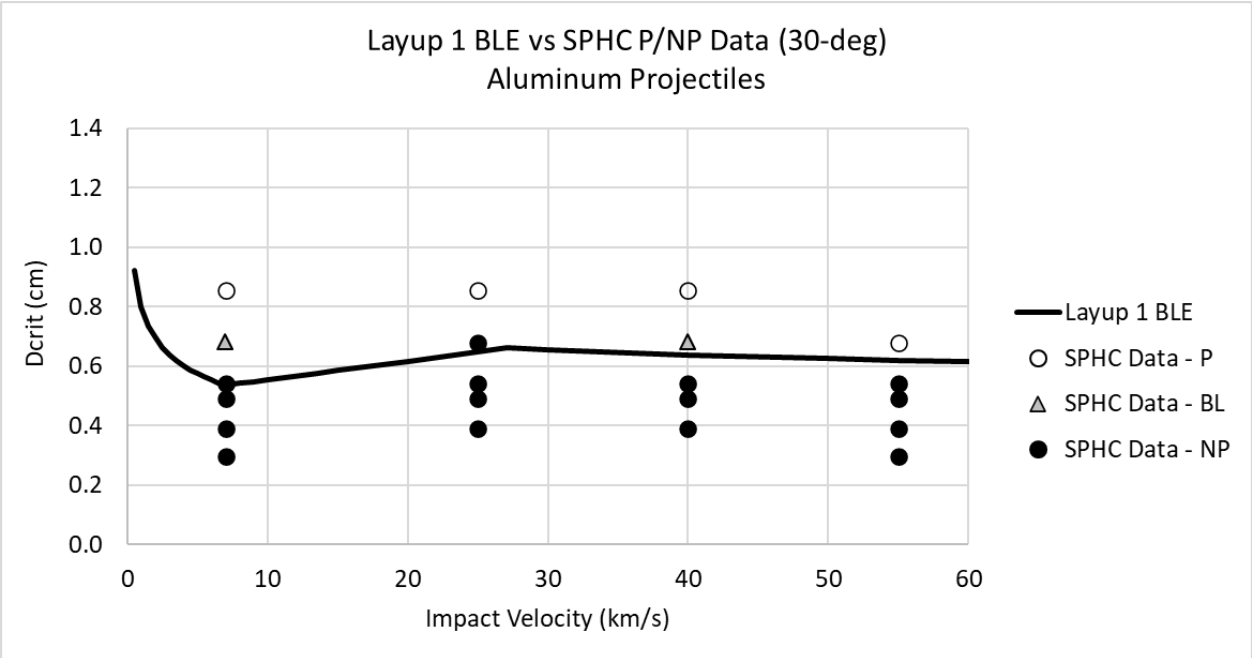

Figure 3. Comparison of MSS+TPS BLE and SPHC Hydrocode Predictions for Layup 1, 30-deg Impacts, Aluminum Projectiles

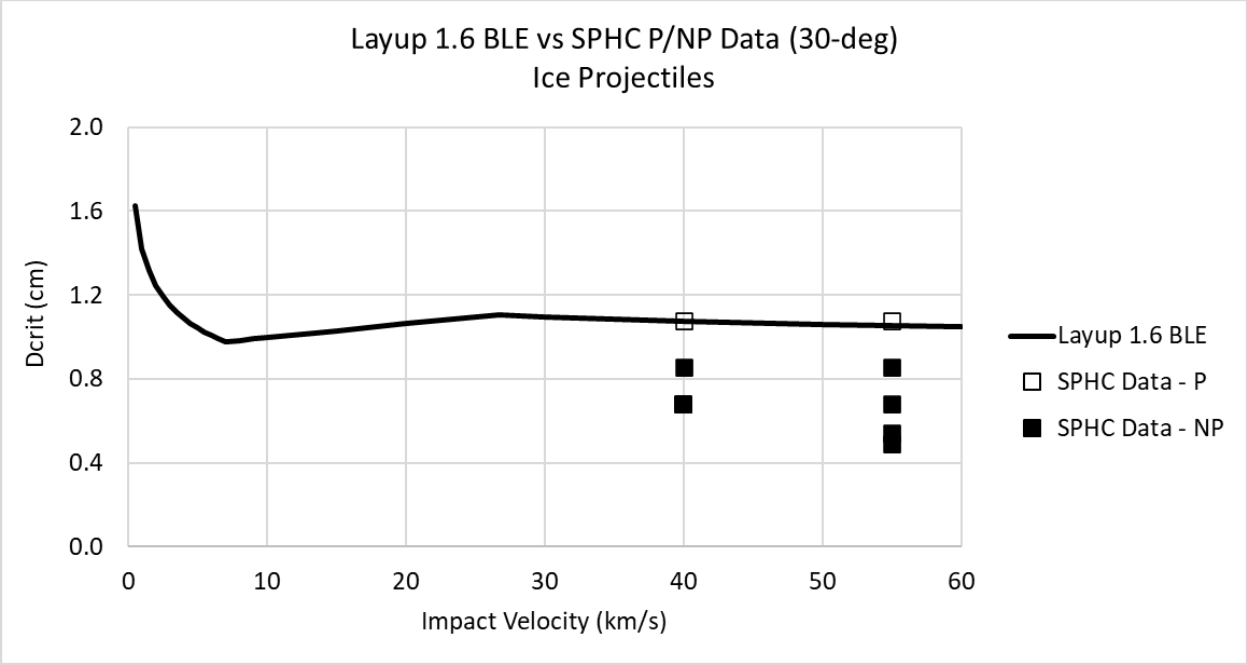

Figure 4. Comparison of MSS+TPS BLE and SHPC Hydrocode Predictions for Layup 1.6, 30-deg Impacts, Ice Projectiles

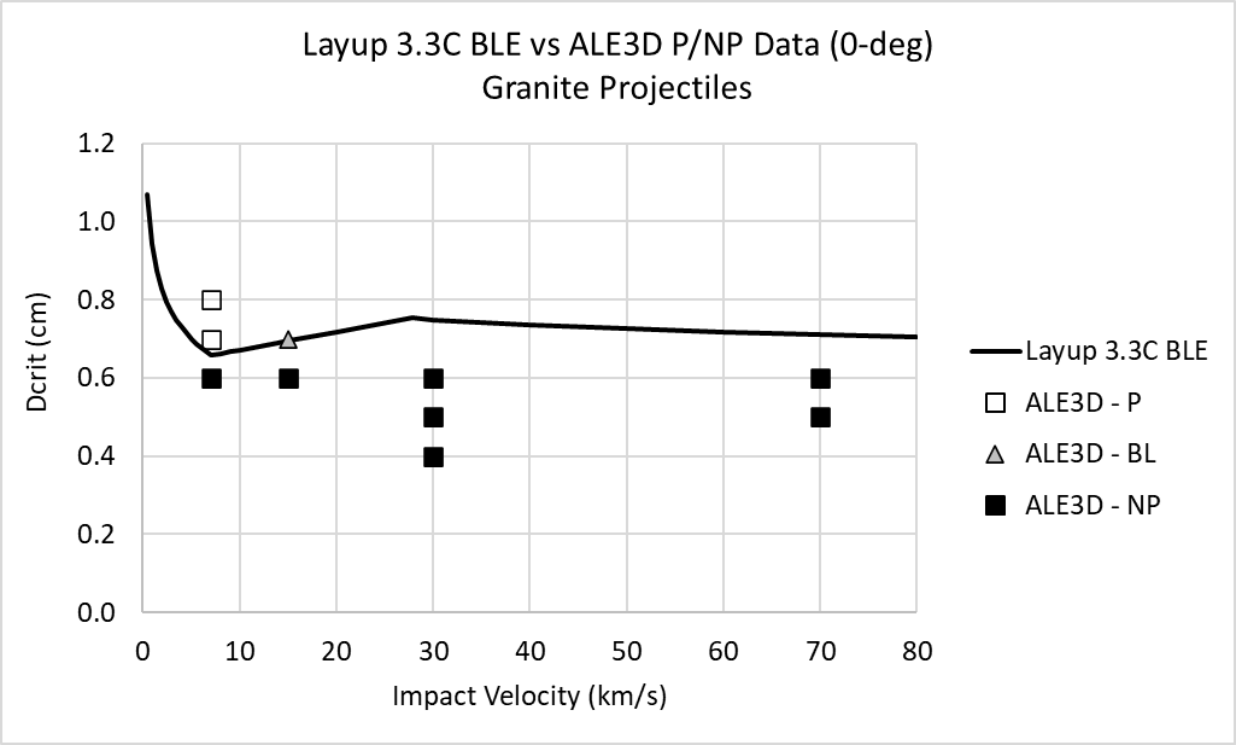

Figure 5. Comparison of MSS+TPS BLE and ALE3D Hydrocode Predictions for Layup L3.3C, 0-deg Impacts, Granite Projectiles

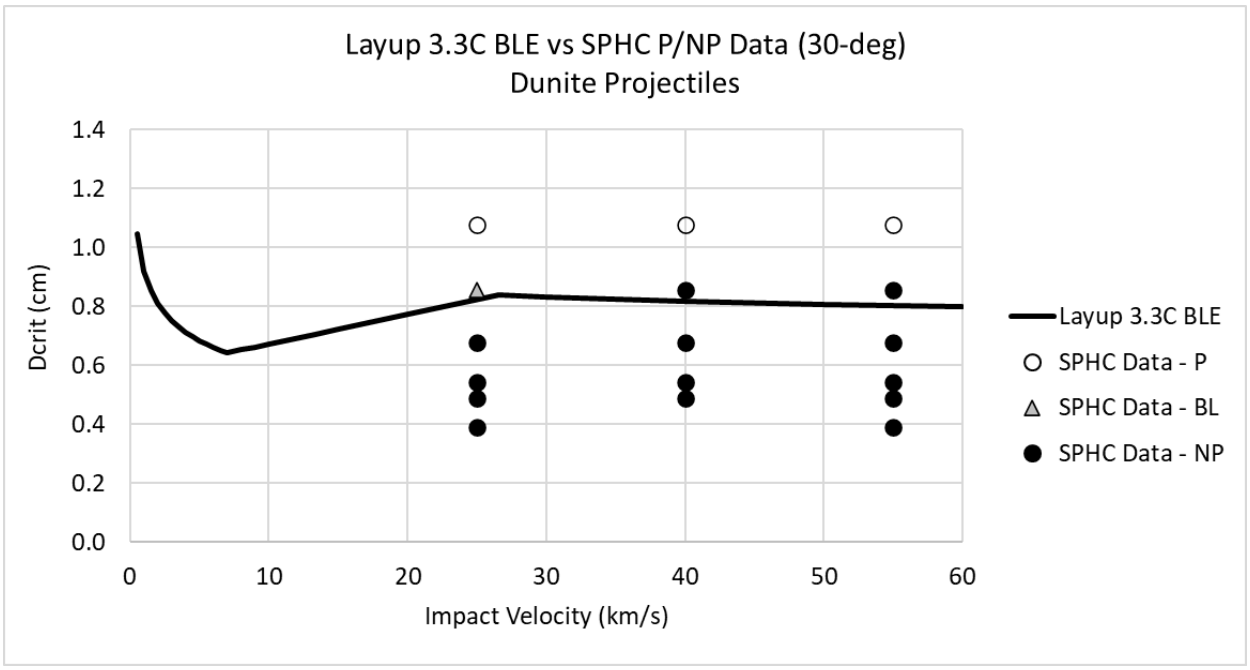

Figure 6. Comparison of MSS+TPS BLE and SPHC Hydrocode Predictions for Layup L3.3C, 30-deg Impacts, Dunite Projectiles

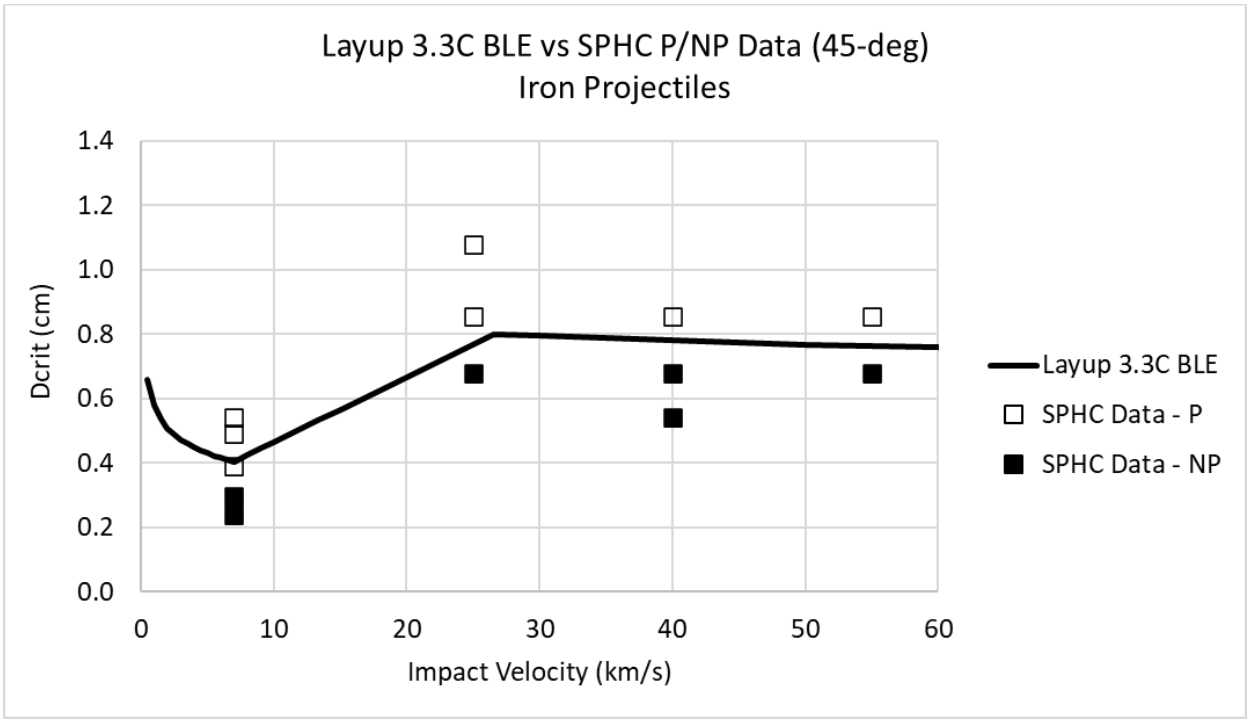

Figure 7. Comparison of MSS+TPS BLE and SPHC Hydrocode Predictions for Layup L3.3C, 45-deg Impacts, Iron Projectiles

Similarly, solid markers below the BLE correspond to hydrocode runs or impact tests without TPS failure with projectiles having diameters smaller than ballistic limit diameters as predicted by the BLE, and also indicate successful MSS+TPS BLE predictions. Conversely, a hollow marker below the BLE line or a solid marker above that line indicates an unsuccessful prediction of the MSS+TPS BLE. This would be the case, for example, if a hydrocode run showed a TPS failure caused by a projectile with a diameter smaller than the ballistic limit diameter as predicted by the MSS+TPS BLE, or a hydrocode run showed a TPS non-failure, but with a projectile having a diameter larger than the predicted ballistic limit diameter.

Figures 2 – 7 are, of course, a representative subset of 31 comparison plots used to adjust and fine tune the exponents and coefficients in Eqns (5-11). In total, these comparison plots indicate that, for the most part, the MSS+TPS BLE slots in quite nicely between the highest NP data points and the lowest P data points for projectile materials, impact velocities, and target configurations considered.

These highly parametric BLEs were developed with flexibility as a priority to allow variations in shield configurations to be explored during an initial sample return spacecraft design phase. This strategy reflected a trade-off for how precisely the BLEs reflected the hydrocode and testing data vs. a high level of flexibility. As spacecraft designs are solidified, priorities will likely shift to creating BLEs that reflect as much as possible the data that go into creating them. This will result in configuration-specific BLEs, only applicable to specified conditions, with unique parameters, exponents, and other terms. The velocity inflection points (i.e., V_H and V_L) would most likely be different for each BLE (instead of held constant as was the case for the BLEs developed herein).

Also of note is that the BLEs developed herein assumed a failure criterion of complete

penetration through the TPS, in other words, penetration through 100% of the TPS thickness. In reality, the failure criterion could depend on which region of the TPS is impacted. Depending on its location on the returning spacecraft, some of the TPS could have a failure criterion of only 50% penetration. In such cases, we expect the BLEs to look similar to the 100% cases, but shifted upward to reflect the fact that smaller particles will be able to create critical damage than those required in the 100% cases.

Finally, in this study we developed a BLE that relied on a failure criterion written in terms of a maximum allowable TPS penetration depth that would be caused by the impact of debris cloud particles exiting the multi-shock shield following an initial high-speed impact. There are, of course, other possible TPS failure modes that may need to be considered, including, for example, allowable material stresses or strains, allowable TPS surface area erosion or total eroded volume, and for whatever kind of damage it sustains, the ability of the TPS to still provide adequate protection to the substructure. Alternative formulations of the BLE can be developed, especially those in which the particular failure criterion being used is an input variable in the BLE. This will allow the effects of different failure criteria on system response to be analyzed, which then can be used to determine whether or not assumed failure mode has any effect on assessed risk for spacecraft using this kind of a protective shielding system.

Conclusions

A particle-impact-based BLE has been successfully developed for TPS that is protected by a multi-shock shield. It was shown to be applicable for projectile densities ranging from 1.0 (i.e., water) to 8.0 g/cm^3 (i.e., steel), impact velocities ranging from 1 to 60 km/s, impact obliquities ranging from 0 to 45 deg (i.e., from normal to highly oblique impacts), and for a

variety of shield component materials, thicknesses, and spacings. Because of the manner in which it was developed (i.e., by considering all relevant material and geometric parameters), the BLE is sufficiently flexible so that it can be used for configuration design trade studies and probabilistic risk assessment exercises. Finally, future work could include extension of the BLE developed herein to different TPS materials, thicknesses, and stand-off distances from the shields to further widen its applicability. Alternative failure criteria like that discussed above can also be considered, especially if the BLE is cast in a form wherein the particular failure criterion being used is included as an input variable of some kind in the BLE.

Acknowledgements

The authors wish to acknowledge the support provided by the NASA Engineering and Safety Center that made this study possible. The authors are also grateful to Eric Christiansen and the NASA teams that performed the high-speed impact tests that were used in the development of the ballistic limit equation presented in this paper.

References

Cataldo, G., Affentranger, L., Clement, B.G., Glavin, D.P., Hughes, D.W., Hall, J., Sarli, B., and Szalai, C.E. 2024. "The planetary protection strategy of Mars Sample Return's Earth Return Orbiter mission", *Journal of Space Safety Engineering*, Vol. 11, No. 2, pp. 374-384 (https://doi.org/10.1016/j.jsse.2024.04.013).

Christiansen, E.L. 1993. "Design and Performance Equations for Advanced Meteoroid and Debris Shields", *International Journal of Impact Engineering*, Vol. 14, pp. 145-156.

(https://doi.org/10.1016/0734-743X(93)90016-Z).

Corbett, B., Williamsen, J., Stellingwerf, R., and Squire. 2024. "Smooth Particle Hydrodynamic Code Predictions for Meteoroid Damage to Thermal Protection Systems Shielded by Composite Structures", *Proceedings of 2024 Hypervelocity Impact Symposium*, 9-13 September, Tsukuba, Japan.

Gerassimenko, M. 1998. "The ALE Advantage in Hypervelocity Impact Calculations", in Proceedings of the 1998 Nuclear Explosives Code Development Conference, Las Vegas, NV, 25-30 October.

Libben, B.J., Needels, J.T., Ellerby, D.T., Vander Kam, J.C., White, T.R. 2019. "High Velocity Impact Performance of a Dual Layer Thermal Protection System for the Mars Sample Return Earth Entry Vehicle", *Proceedings of the 16th International Planetary Probe Workshop (IPPW)*, Oxford University, UK, 8-12 July.

Miers, K.T., Al-Shehab, N.M., and Pudlak, D.J. 2020. "High Pressure Oblique Shock Interactions in NATO Fragment Impacts", *in* Proceedings of the Conference of the American Physical Society Topical Group on Shock Compression of Condensed Matter, 16–21 June 2019, Portland, OR, AIP Conference Proceedings, Vol. 2272, Paper No. 120016.

Noble, C., Anderson, A., Barton, N., Bramwell, J., Capps, A., Chang, M., Chou, J., Dawson, D., Diana, E., Dunn, T., Faux, D., Fisher, A., Greene, P., Heinz, I., Kanarska, Y., Khairallah, S., Liu,

548 B., Margraf, J., Nichols, A., and White, J. 2017. ALE3D: An Arbitrary Lagrangian-Eulerian
549 Multi-Physics Code, Report No. LLNL-TR-732040, Lawrence Livermore National Laboratory,
550 CA.
551
552 Sarli, B., Bowman, E., Cataldo, G., Feehan, B., Green, T., Gough, K., Hagedorn, A., Hudgins,
553 P., Lin, J., Neuman, M., Parvez, E., Rondey, J., Szalai, C., and Yew, C. 2024. "NASA's Capture,
554 Containment, and Return System: Bringing Mars samples to Earth", *Acta Astronautica*, Vol.
555 223, pp. 270-303.
556
557 Schonberg, W.P. 2016. "Concise History of Ballistic Limit Equations for Multi-Wall Spacecraft
558 Shielding", *Reviews in Human Space Exploration*, Vol. 1, No. 1, pp. 46-54.
559
560 Schonberg, W.P., and Squire, M.D. 2024. "Analyzing Micrometeoroid and Orbital Debris Shield
561 Performance for Sample Return Spacecraft", *Journal of Spacecraft and Rockets*, available
562 online, 05 June 2024 (https://doi.org/10.2514/1.A35997).
563
564 Schonberg, W.P, and Williamsen, J. 2023. "Characterizing the Largest Debris Cloud Particle
565 Created by Thin Plate Impact", *Journal of Spacecraft and Rockets*, Vol. 60, No. 2, pp. 375-380
566 (https://doi.org/10.2514/1.A35491).
567
568 Stellingwerf, R.F. 1990. "Smooth Particle Hydrodynamics", *in* Advances in the Free-Lagrange
569 Method: Proceedings of the Next Free–Lagrange Conference, *eds.* H.E. Trease, M.J. Fritts, and
570 W.P. Crowley, Springer Verlag, pp. 239-247.

Stellingwerf, R.F., and Wingate, C.A. 1994. “Impact Modeling with Smooth Particle Hydro-dynamics,” *Journal of the Italian Astronomical Society*, Vol. 65, pp. 1117-1128.

Wilbeck, J.S., Herwig, S.B., Kilpatrick, J.M., Faux, D.R., Weir, R.J., Hertel, E.S., and Dutta, M.K. 2001. “Hypervelocity Impact of Spaced Plates by a Mock Kill Vehicle”, *International Journal of Impact Engineering*, Vol. 26, pp. 853-864 (https://doi.org/10.1016/S0734-43X(01)00139-7).

Williamsen, J., Stellingwerf, R., Evans, S., and Squire, M. 2022. “Prediction and Enhancement of Thermal Protection Systems from Meteoroid Damage using a Smooth Particle Hydro-dynamics Code”, *Proceedings of 2022 Hypervelocity Impact Symposium*, 18-22 September, Alexandria, VA (https://doi.org/10.1115/HVIS2022-59).

Wingate, C.A., Stellingwerf, R.F., Davidson, R.F., and Burkett, M.W. 1993. “Models of High Velocity Impact Phenomena”, *International Journal of Impact Engineering*, Vol. 14, pp. 819-830.